Title

The synergistic effect of micro-topography and biochemical culture environment to promote angiogenesis and osteogenic differentiation of human mesenchymal stem cells

Authors

Shang Song[a], Eun Jung Kim[a], Chelsea S. Bahney[b], Theodore Miclau[b], Ralph Marcucio[b], Shuvo Roy[a,*]

[a] Department of Bioengineering and Therapeutic Sciences, University of California - San Francisco, San Francisco, CA, 94158, United States

[b] Department of Trauma Institute, University of California - San Francisco and San Francisco General Hospital, San Francisco, CA, 94110, United States

* Corresponding author: Department of Bioengineering and Therapeutic Sciences, University of California - San Francisco, Byers Hall, Room 203A, MC 2520, 1700 4th Street, San Francisco, CA 94158, USA.

E-mail address: shuvo.roy@ucsf.edu (S.Roy)

Phone number: 415-514-9666

Fax number: 415-514-9766

1. Introduction

Bone is the second most common transplanted tissue [1, 2] with an estimated 2.2 million grafting procedures performed annually worldwide [3]. The gold standard for bone regeneration is to use autologous bone grafts for traumatic injuries, fracture non-unions, spinal fusion, and hip joint replacements, and other bone-related diseases [4]. However, autologous grafting is associated with limited availability of donor tissue for clinical applications [5-7] and significant patient morbidity and complication rates of 8.6%-20.6% [1, 8, 9]. Allograft technologies have been developed to address the limited availability of autograft bone. However, the process of decellularization, sterilization, and allograft storage disrupts the osteoinductive nature of the tissue and results in clinical failure rates of 16-35% predominantly due to the inability of these grafts to adequately re-vascularize [10, 11]. As such, there is a significant and growing need for strategies to promote vascularized bone graft substitutes for this unmet clinical need. Several strategies have been used to stimulate musculoskeletal healing, such as controlled release of growth factors to promote vascularization [12-15] or regulation of osteogenesis with mechanical properties [16-21]. Nonetheless, the lack of host vasculature penetration and integration between engineered bone scaffold constructs and host tissue still remains a fundamental challenge during bone fracture healing [22-24]. An understanding of the scaffold's underlying physical properties and its biochemical environment is crucial to elicit the desired biological responses for bone regeneration [25, 26].

Surface topographical characteristics are important aspects in designing biological implants, as they have great implications in cell guidance and behavior [27-35]. The development of microfabrication and related microelectromechanical systems (MEMS) technologies such as soft lithography offers unprecedented reproducibility and precision to create surface topography that can interact with cells and tissues in a systematic manner [36-39]. For instance, Dalby *et al.* demonstrated that different arrangements of topographical disorder could modulate osteogenic differentiation of human mesenchymal stem cells (hMSCs) [40]. The Chen group demonstrated that the inherent rigidity of different sized micropatterns could shift the balance of hMSC fates, alternating between osteogenesis and adipogenesis [41, 42]. Our laboratory also reported that 10 μm diameter post microtextures on polydimethylsiloxane (PDMS) significantly increased proliferation and osteogenesis of human bone

marrow-derived connective tissue progenitor cells (CTPs) compared with those cultured on smooth surface [21, 43]. These results suggest that varying geometry and arrangement of the surface topography can result in the modification of cell proliferation and morphology as well as the potential to enhance lineage specificity. However, there has been little investigation on the synergistic effects of microscale surface topography and biochemical attributes for tuning hMSC fate in vivo. Particularly, in vivo studies concerning microtextured materials have demonstrated mixed results in which microgrooved surfaces produced the same cellular and tissue response as smooth surfaces [44, 45]. It has been suggested that an amorphous layer was formed between the surface microtexture and the connective tissue due to the influence of inflammatory cells present at the site of implant surface. Hence, cells from the connective tissue were unable to sense and respond to the micro-topograhy [44, 46].

The goal of this study is to evaluate the long-term combined effect of microtextured topography and biochemical cues on hMSC proliferation and osteogenic differentiation, and re-vascularization in mice for potential bone tissue engineering applications. Specifically, PDMS substrates with 10 μm cylindrical post (diameter, height, and interspace) were created to culture hMSCs for 6 weeks under two different conditions: 1) one group in the proliferative basal medium (BM) during the entire study; 2) another group in the BM for the first five weeks and in the differentiative osteogenic medium (OM) for the last week. The in vitro pre-culture maximized material-cell interaction for lineage specificity on microtextured scaffolds, ensuring adequate hMSCs sensing and response to topographical signals for in vivo development. The in vivo study investigated the potential osteogenic differentiation and vascular integration of hMSCs with the host environment by subcutaneous implantation of hMSCs on microtextured substrates in BM and OM for 6 weeks.

2. Materials and Methods

2.1 Experimental Design

Bone marrow derived hMSCs were cultured for 6 weeks on 10 μm micropost PDMS substrates under two conditions: 1) in the proliferative basal medium (BM) during the entire study, and 2) in the BM for the first five weeks and in the differentiative osteogenic medium (OM) for the last week. Cell seeded scaffolds were analyzed in vitro using fluorescent microscopy, scanning electron microscopy (SEM),

histological stains, and real time polymerase chain reaction (RT-PCR). Cell seeded scaffolds were also subcutaneously implanted into mice for 6 weeks.

2.2 In vitro evaluation of hMSCs cultured on microtextured substrates

2.2.1 Fabrication of microtextured substrates

The microfabricated-patterned mold was prepared using soft lithography techniques as previously described (Fig. 1) [43]. To prepare the PDMS substrate, liquid PDMS base and curing agent (Sylgard 184; Dow Corning) were mixed at a ratio of 10:1, degassed, and poured uniformly on top of the patterned mold. After curing the patterned mold at 85 ℃ for 2 h, solidified PDMS casts with 10 μm cylindrical posts were released from the mold (Fig. 3,a). Patterned PDMS substrates were cut into 4 mm diameter disks, sterilized for 30 min with 70 % ethanol, and washed 3 times with phosphate buffered saline (PBS) for subsequent cell culture.

2.2.2 Cell culture

Human MSCs (PT-2501, Lonza, Allendale, NJ) were cultured on microtextured 4 mm disks under standard culture conditions. For the BM condition, hMSCs seeded on microtextured PDMS scaffolds were grown in Dulbecco's modified Eagle's medium (DMEM) low glucose (CCFAA001, UCSF Cell Culture Facility) supplemented with 10% fetal bovine serum (FBS) (Life Technologies), 1% penicillin-streptomycin (P/S) (CCFGK003, UCSF Cell Culture Facility), and 10 ng/mL recombinant human FGF-2 (R&D Systems, Minneapolis, MN) for 6 weeks. For the OM condition, hMSCs seeded on PDMS substrates were first grown under BM for 5 weeks before exposed to osteogenic media (OM) in DMEM high glucose (CCFAA005, UCSF Cell Culture Facility) supplemented with dexamethasone (10^{-7} M) (D4902, Sigma), L-Ascorbic acid 2-phosphate (100 μM) (A8960, Sigma), β-glycerol phosphate (10 mM) (50020, Sigma), sodium pyruvate (100X) (CCFGE001, UCSF Cell Culture Facility), ITS+ (BD Biosciences, NJ), and 1% P/S for another week. Seeding density for both conditions was $2X10^6$ cells/cm^2.

Mouse preosteoblast cell lines MC3T3 (obtained from R.Franceschi, University of Michigan, Ann Arbor, MI) and calB 2T3 (obtained from S.E.Harris, University of Texas, San Antonio, TX) were cultured on microtextured substrates as positive controls. For the BM condition, they were grown on microtextured PDMS scaffolds in α- Minimum Essential Medium w/o nucleosides (α-MEM) (CCFAC006, UCSF Cell Culture Facility), 10% FBS, and 1% P/S. For the OM condition, they were moved to OM comprising α-

MEM, 2% FBS, L-Ascorbic acid 2-phosphate (10 µg/mL), β-glycerol phosphate (10 mM), and 1% P/S. Seeding density for both conditions was $2X10^6$ cells/cm^2.

For all data shown, hMSCs were used between passages 5-7. MC3T3 and calB2T3 were used between passages 12-16 and passages 15-25, respectively. Individual experiments were repeated at least 3 times with different cell preparations.

2.2.3 Cell proliferation and morphology

After cells were cultivated for 6 weeks on microtextured substrates, the media was removed and washed with PBS. For the proliferation study, they were stained with 0.4% trypan blue and counted. For morphology observation, they were fixed in a solution containing 3 % glutaraldehyde (G7651, Sigma), 1M sodium cacodylate (Polysicences) and 0.1M sucrose (Sigma). After 2 days, the substrates were washed with distilled water. Dehydration was achieved by placing these scaffolds in an increasing concentration of ethanol (50-100%). Dehydrated samples were then mounted on aluminum stubs, sputter-coated with gold-palladium, and examined with SEM (Ultra 55, Carl Zeiss).

2.2.4 Quantitative gene expression

Total RNA of hMSCs from different conditions was extracted using the RNeasy® Mini Kit (Qiagen). The quantity of the RNA was determined using NanoDrop™ ND-1000 spectrophotometer (NanoDrop Technologies, DE, US). cDNA was obtained using 100 ng of total RNA plus master mix from Fast SYBR® Green Cells-to-CT™ Kit (Life Technologies) with BioRad iCycler (BioRad, CA). Real-time quantitative reverse transcription polymerase chain reaction (RT-PCR) was performed using 7900HT PCR system (Applied Biosystems) and Fast SYBR Green PCR kit (Life Technologies). For in vitro cell-based scaffolds, relative quantification of human Collagen X (COL X), Collagen I (COL I), Alkaline Phosphatase (ALP), Bone Sialoprotein (BSP), Osteocalcin (OC), Collagen II (COL II), and Peroxisome Proliferators-Activator Receptor γ (PPARγ) was performed using the comparative C_T (crossing of threshold) method ($\Delta\Delta C_T$ method) [47] with GAPDH from hMSCs cultured on smooth surface and human osteosarcoma cell line Saos-2 cultured on smooth surface as negative and positive controls, respectively. Primers (IDT Technologies) used in this study were previously published sequences (Table 1). In vivo scaffolds were also analyzed with previous mentioned markers. Relative quantification of mouse platelet endothelial cell adhesion molecule (PECAM) and mouse vascular endothelial growth factor (VEGF)

(Table 2) were analyzed with mouse GAPDH used as an internal control and no cDNA used as a negative control. Each experiment was performed at least in triplicate.

2.2.5 Immunofluorescence of bone-specific markers

Cells on microtextured substrates were fixed with 4% formaldehyde followed by PBS washes, permeabilized with 0.1% Triton X-100 for 10 min, and incubated in blocking solution (PBS, 1% bovine serum albumin (BSA)) for 30 min. Samples were incubated with primary antibodies (COL IA: sc-8783, OC: sc-30044; Santa Cruz Biotechnology) at a dilution of 1:200 for 1 hr and washed twice for 5 min with PBS to remove residues. Another incubation with secondary antibodies (COL1A: anti-goat sc-2783, Santa Cruz Biotechnology; OC: anti-rabbit A-21206, Life Technologies) at a dilution of 1:500 for 1 hr was used followed by PBS washes for 5 min. DAPI (Vectashield) was added for nuclear staining. Images were obtained using 6D High Throughput Perfect Focus System (Nikon Instruments) for in vitro scaffolds (Fig. S1). In vivo scaffolds (Fig. 9 &10) were analyzed with laser scanning spectral C1si confocal microscope (Nikon Instruments).

2.2.6 Mineral content

Quantitative analysis of ALP activity was performed as previously described [48], using Sigma Fast p-nitrophenyl phosphate tablet sets (Sigma). Cell seeded scaffolds were washed with PBS, then substrate buffer made from p-nitrophenyl phosphate tablet sets were added to each sample. After 10 min, NaOH was added to supernatants taken from each sample to stop enzymatic activity. ALP activity was measured by Spectra Max M2 plate reader (Molecular Devices) at 405 nm using p-nitrophenyl as a standard and analyzed according to the manufacturer's protocol (85L-3R, Sigma).

2.2.7 Calcium deposition

Samples were fixed with 70% ethanol at room temperature for 15 min. After washes with distilled water for 5 min, 1% alizarin red stain (Sigma) was added to samples for 20 min. Samples were washed with distilled water 4 times. Images were obtained using Leica DFC 295 (Leica Microsystems).

2.2.8 Histology

Hall Brunt Quadruple stain [49] was used to distinguish bone (red) from cartilage (blue). Samples were fixed with 70% ethanol. They were stained with 0.5% celestine blue solution (51050, Fisher Scientific) consisted of 14% glycerin and 5% ammonium sulphate) for 5 min, Mayer's haematoxylin

(75290, Fluka) for 5 min, 1% alcian blue in 1% acetic acid (74240, Merckmillipore) for 6 min, 1% phosphomolybdic acid for 1 min, and 0.5% direct red solution (28160, Polysicences) for 6 min. Samples were washed with distilled water for 2-5 min between each stain. Images were obtained using Leica DFC 295 (Leica Microsystems).

2.3 In vivo animal studies

All animal studies were approved by the UCSF IACUC. Immunocompromised nude mice (Homozygus Nu/J strain #002019; Jackson Laboratories, Sacramento CA) were used for transplantation in order to prevent any graft rejection. A total of 6 adult male mice (9-14 weeks old) were anesthetized with an intraperitoneal injection of 1.5 mg ketamine and 0.15 mg medetomidine. The skin was cleaned with povidone-iodine and chlorhexidine gluconate (4% w/v). Using a scalpel or surgical scissors, 1-2 mm incisions were created in the skin on the dorsal side of the mice approximately 10-15 mm from the midline. Subcutaneous pockets were generated in the connective tissue beneath the incision using blunt dissection and scaffolds were placed at least 1 mm laterally from the incision site with the printed scaffold features facing the subcutis. Each mouse received 8 scaffolds. Scaffolds were placed approximately 20 mm from each other in a linear fashion, dorsal to caudal, such that scaffolds are sufficiently isolated from each other. The incisions were closed with two 6.0 silk sutures and covered with a triple antibiotic ointment. Anesthesia was reversed and animals were provided with post-surgical analgesics per approved protocol. Animals were socially housed, allowed to ambulate freely, and survived for 6 weeks prior to cellular and molecular analyses. We have previously found that this protocol is well tolerated by the animals.

Three types of scaffolds were prepared by methods described in previous section (2.2.2) for transplantation: 1) microtextured PDMS without cells, 2) hMSCs on microtextured PDMS in BM, and 3) hMSCs on microtextured PDMS in OM. Harvested scaffolds were analyzed using methods illustrated previously in this section (2.2.3-2.2.8).

2.3.1 Immunofluorescence of angiogenic marker

In vivo scaffolds were fixed using same procedure in section 2.2.5. Primary antibodies anti-human mitochondria (MAB1273, Millipore) with 1:10 dilution and anti-mouse PECAM-1 (B&D Biosciences) with 1:200 dilution were used. Secondary antibodies anti-rat (A-11006, Life Technologies) and anti-mouse

(A-11014, Life Technologies) were used to incubate harvested scaffolds. DAPI was added for nuclear staining. Images were obtained using laser scanning spectral C1si confocal microscope (Nikon Instruments).

2.3.2 Histology

Harvested scaffolds were fixed in 4% paraformaldehyde for 15 min and processed to paraffin using standard protocols. Sections were cut at 5 µm and mounted on glass slides. Hematoxylin and Eosin (HE) was performed on the subsequent slides. Slides were deparafinized using 3 changes of xylene for 2 min, rehydrated through a graded ethanol series (100%, 95%, 70%) each for 1 min. Slides were washed in water followed by 7 min in Mayers Haematoxylin to stain nuclei (HXMMHGAL, American Mastertech). Excess haematoxylin was removed with water for 1 min followed by bluing (HXB00242E, American Mastertech) for 1 min. Excess bluing was removed with water for 1 min. Slides were then placed in 70% ethanol for 1 min and Eosin/Phloxine were used to stain cytoplasm and connective tissues (STE0457, American Mastertech). Eosin was differentiated for 1 min in 95% alcohol and the tissue sections are dehydrated in 2 changes of 100% alcohol followed by 3 changes of 2 min in xylene and mounted in a resinous based mounting media (361254D Depex, Fisher Scientific). Slides were dried and viewed under Leica DFC 295 (Leica Microsystems).

2.4 Statistical Analysis

Sample pairs were analyzed by the Student's t-test. Multiple samples were evaluated with one way or two way analysis of variance (ANOVA) followed by Bonferroni and multiple comparison using Prism (San Diego, CA). A P value of <0.05 was accepted as statistically significant for all samples.

3. Results

3.1 In vitro culture analysis

3.1.1 Cell proliferation and morphology

The microtextured PDMS disks cultured with hMSCs exhibited a higher proliferative capacity in BM than OM after a 6-week culture period (Fig. 2). Positive control mouse pre-osteoblast cell lines calB2T3 and MC3T3 demonstrated significantly more cell growth in both BM and OM compared with that of the hMSCs (Fig. 2). The SEM images also revealed that hMSCs tended to attach onto cylindrical posts by spreading their processes to other posts and neighboring cells in BM (Fig. 3,b), whereas hMSCs

cultured in OM condition displayed layers of ECM that covered most of the microtextured surfaces (Fig. 3,c).

3.1.2 Gene and extracellular matrix protein (ECM) expression

The expression of osteoblast-specific markers was assessed in hMSCs on microtextured substrates under BM and OM conditions in vitro using real time RT-PCR (Fig. 4). Findings indicated that hMSCs on microtextured substrates differentiated toward osteogenic lineage even when cultured under proliferative BM condition as shown by the relative expression of osteoblast-specific markers (COL I, ALP, BSP, and OC) (Fig 4,a). The osteogenic capacity of hMSCs on microtextured substrates in BM was significantly elevated by switching to OM as indicated by a 5.5-to-6 fold increase in COL I, 2.7-fold increase in ALP, 1.3-to-1.7 fold increase in BSP, and 1.6-fold increase in OC (Fig 4). The chondrogenic and adipogenic markers (COL II and PPARγ) were not expressed (Fig 4,a).

The osteogenic differentiation of hMSCs on microtextured substrates was also confirmed by immunohistological detection of osteoblast markers COL I and OC. Human MSCs on microtextured substrates in both BM and OM showed a greater intensity of osteoblast markers compared with hMSCs on smooth surfaces (Fig. S1).

3.1.3 Histological analysis of hMSCs on microtextured substrates

Direct visualization of mineralization and calcium deposition verified bone cell differentiation and bone formation. The hMSCs on microtextured substrates in OM possessed a significant increase in ALP activity compared with cells in BM (Fig. 5). Results from alizarin red data indicated that hMSCs on microtextured substrates stained more intensely in OM than BM (Fig. S2). Overall, the spatial distribution and intensity of both alizarin red stain were found to be consistently greater for cells cultured in OM than BM.

3.2 In vivo animal study

3.2.1 Scaffold morphology

After a 6-week implantation period in the mice, harvested scaffolds displayed various levels of vascularization, which we observed during the explant process (Fig. 6) (Table 3). Generally, hMSCs on microtextured substrates in OM showed a more extensive vascular invasion throughout the entire scaffold (Fig. 6(c,d)), while hMSCs on post microtexture in BM exhibited vascularization mostly on the edge of the

scaffolds (Fig. 6,b). Minimal vasculature was observed in the microtextured substrates without hMSCs (Fig. 6,a). SEM images demonstrated that all implanted scaffolds developed ECM rich capsules with uniform shape and thickness around the entire microtextured substrates (Fig. 7). However, the sprouting of new blood vessels [50] in tissues surrounding the implants was significantly higher for hMSCs on microtextured substrates in OM (Fig. 7(e,f)) compared with microtextured substrates without hMSCs (Fig. 7(a,b)) and hMSCs on microtextured substrates in BM (Fig. 7(c,d)).

3.2.2 Gene and ECM expression

The expression of osteoblast-specific markers was assessed in harvested scaffolds using quantitative RT-PCR (Fig. 8,a). Similar to the gene analysis results in vitro, hMSCs on microtextured substrates in BM differentiated toward osteogenic lineage with increased expression of osteoblast-specific markers (ALP, BSP, and OC) (Fig. 8,a). Compared with hMSCs on microtextured substrates in BM, the osteogenic capacity of hMSCs on microtextured substrates in OM was expedited as shown by a 4-fold increase in COL I, 3.3-fold increase in ALP, 2.2-fold increase in BSP, and maintained a constant level of OC expression (Fig. 8,a). The chondrogenic and adipogenic markers (COL II and PPARγ) were not expressed (Fig 8,a). The synergistic effects of microtextured surfaces and the OM enhanced osteogenesis of hMSCs in vivo. The expression of angiogenic genes showed that PECAM and VEGF were 5.8- and 58.7-fold higher in hMSCs on microtextured substrates in OM compared with BM, suggesting that both the microtopology and growth-factor induction contribute to angiogenic capacity of this system (Fig. 8,b).

The osteogenic differentiation of harvested scaffolds was further confirmed by the immunohistochemistry of COL I and OC. Both hMSCs on microtextured substrates in BM and OM exhibited high intensity of COL I and OC (Fig. 9). The vascularization of harvested scaffolds was observed using mouse PECAM (Fig. 10). Although microtextured substrates showed minimal cell attachment and lacked any vasculature, hMSCs on microtextured substrates in both BM and OM confirmed the presence of hMSCs and demonstrated vascularization to various degrees (Fig. 10).

3.2.3 Histological analysis

The ALP activity of harvested scaffolds was comparable between hMSCs on microtextured substrates in BM (116 mU/L) and OM (120 mU/L) (Fig. 11). Microtextured substrates alone exhibited ALP

activity of 65 mU/L, which was significantly lower compared with PDMS substrates that were cultured with cells (BM and OM), probably due to non-specific cell attachment to the substrate surfaces over the period of in vivo implantation. Alizarin red results showed that hMSCs on microtextured substrates in both BM and OM were stained more intensely compared with microtextured substrates, indicating improved calcium deposition from bone matrix formation (Fig. S3). HE stain showed densely nucleated epithelial layers surrounding the scaffolds for hMSCs on microtextured substrates in BM (Fig. 12,b) (Fig. S4,a), whereas loose epithelial layers with extensive blood vessels were identified for hMSCs on microtextured substrates in OM (Fig. 12,c-e) (Fig. S4,b). Blood was also detected in the vascular lumen of hMSCs on microtextured substrates in OM (Fig. 12,c-e).

4. Discussion

Bone regeneration and repair require the coordination of multiple cellular processes, the first of which is the migration, proliferation, and differentiation of osteoprogenitors [51]. This process is regulated in part by soluble and adhesive factors from ECM that bind to cell surface receptors, but recent advances suggest that the mechanical properties of the ECM also play an important role in mediating cell signaling, migration, proliferation, and differentiation [52, 53]. Therefore, to better mimic the natural environment of the cells, synergistic effects of mechanical, chemical, and topographical cues at the micro- and nanoscale is necessary to modulate specific cell function [54, 55]. We postulate that the osteogenic differentiation of hMSCs can be optimized both in vitro and in vivo with a combined effect from topographical cues based on post microtexture design and biochemical supplements. Our group previously demonstrated that microposts with 10 µm in diameter, height, and interspace provide the greatest cell-surface contact area, longer residence time to establish adhesive contacts and corresponding cell proliferation [21, 43]. In the present study, we assessed the ability of 10 µm microposts in two different conditioning medium (BM & OM), independently of surface chemistry, to influence hMSC morphology, proliferation, and osteogenic differentiation in vitro and in vivo.

The number of hMSCs that remained on the substrates after 6 weeks did not change significantly compared with the initial seeding density. This was probably due to the poor cell adhesion properties of PDMS [56] which could reduce initial cell attachment and affect subsequent cell proliferation for long-term studies. The proliferation (Fig. 2) analysis demonstrated that the cells on microtextured substrates were

more proliferative in BM than OM. Cells on microtextured substrates in BM showed excellent attachment, spreading and even distribution on the substrate surface (Fig. 3). Cells on microtextured substrates in OM exhibited dense layers of matrix coverage on the substrate surface. Since the surface topography and surface chemistry of underlying substrates were identical, these results suggest that the BM condition helped the growth of hMSCs, whereas the OM condition deposited more ECM proteins for matrix support. Such effect is contributed by the different biomolecular components of the culture medium: serum and growth factor in BM support the proliferation of hMSCs, but the presence of dexamethasone, ascorbic acid and β-glycerol phosphate in OM induce the differentiation of hMSCs.

A group of osteoblast-specific markers based on the model of osteoblast differentiation demonstrated by Stein and Lian [57] was used to assess different stages of osteogenic differentiation of hMSCs on microtextured substrates in BM and OM conditions (Fig. 4). We found that hMSCs on microtextured substrates in OM showed an increased level of COL I compared with BM (Fig. 4(a,b)), suggesting the early matrix formation for hMSCs stimulated by osteogenic factors [58]. Despite culturing in BM, hMSCs on microtextured surface differentiated into osteogenic lineage, as evidenced by the increase in osteoblast-specific markers such as ALP, BSP, and OC (Fig. 4(a,b)). The addition of OM further elevated the expression of these markers with negligible chondrogenic expression (COL II), indicating hMSCs on microtextured surfaces undergo a direct and specific osteogenesis. The substantial amount of ALP from hMSCs on microtextured substrates in BM and OM (Fig. 4(a,b)) was observed which signified the ECM maturation post proliferative period [59, 60]. The increased levels of BSP and OC (Fig. 4) indicated final stage of extracellular-matrix mineralization [59, 60]. Our data showed that the addition of OM significantly augmented the osteogenic capability of hMSCs on microtextured substrates during each stage of differentiation (Fig. 4). More importantly, the expression level of late stage makers for matrix mineralization process (BSP & OC) were greatly improved compared with those involved during matrix maturation (COL I) (Fig. 4(a,b)). The combined osteoinductive effects from topography and biochemical cues far exceeded that of using either one alone (Fig. 4). Additional verification from immunofluorescence staining of COL I and OC (Fig. S1), quantitative measurement of ALP (Fig. 5), and calcium deposition from alizarin red (Fig. S2) all confirmed osteogenic differentiation of hMSCs with adequate matrix deposition and maturation. These results suggest that the combination of microtextured surfaces and

differentiation factors provided by the OM significantly improve osteogenic differentiation and mineralization of hMSCs in vitro.

To further assess the osteogenic differentiation of hMSCs on microtextured surfaces, scaffolds consisting of microtextured substrates without cells, hMSCs on microtextured substrates in BM, and hMSCs on microtextured substrates in OM were implanted subcutaneously in mice for 6 weeks. Gene expression analysis showed that hMSCs on microtextured substrates in OM exhibited higher levels of COL I, ALP, and BSP compared with BM, suggesting that pre-culture in OM is more effective in promoting hMSCs osteogenic differentiation in vivo (Fig. 8,a). The expression of OC, a marker of late-stage matrix mineralization was expressed equally in hMSCs on microtextured substrates in OM and BM (Fig. 8,a). In vivo matrix maturation, mineralization, and bone formation was further analyzed with ALP (Fig. 11) and alizarin red (Fig. S3). Both hMSCs on microtextured substrates in BM and OM showed significant ALP activity, extensive calcium deposition, and substantial amount of bone matrix formation. The ALP activity was also observed in microtextured substrates without cells (Fig. 11), which was probably a non-specific catalytic and enzymatic activity due to the invasion of subepithelial connective tissues of the animals into scaffolds [61]. Clearly, the differentiative OM condition accelerates the number of hMSCs into early osteoblast differentiation in vivo. However, the osteogenic phenotype of the hMScs pre-cultured under BM suggests that the in vivo microenvironment was sufficient to enable these constructs to promote osteogenesis and mineralization.

We observed that hMSCs on microtextured substrates in OM showed a more expansive local microvasculature around the implants, whereas hMSCs on microtextured substrates in BM displayed some level of vascularization on the edge of the scaffolds, and microtextured substrates alone exhibited no vascularization at all (Fig. 6,10,12) (Table 3). We discovered abundant blood vessels in tissues surrounding the implants as well as regions with clusters of red blood cells for scaffolds consisted of hMSCs on microtextured substrates in OM (Fig. 7(e,f)). This observation was further confirmed by the high level of expression in mouse vascular-specific markers PECAM and VEGF (Fig. 8,b). Immunofluorescence staining showed that individual endothelial cells scattered around the scaffolds (Fig. 10). Observation of mouse angiogenic-related markers implied that the endothelial cells were recruited from the host. Based on the evidence of invasion of host capillaries into the cell-based scaffolds, the

appearance and differentiation of hMSCs into mature osteoblasts, and the lack of chondrogenic expression (COL II) in vivo (Fig. 8,a), we speculated that the implanted hMSCs on microtextured substrates in OM underwent an intramembraneous ossification process [62]. Cells on microtextured substrates in BM demonstrated dense nucleated epithelial-like tissue layers, whereas hMSCs on microtextured substrates in OM exhibited very loose tissue structure occupied with numerous blood vessels (Fig. 12). The formation of blood vessels for scaffolds consisted of hMSCs on microtextured substrates in OM establishes mass transport between the body and the implanted microtextured scaffolds [63]. Past reports have suggested that hMSCs, without differentiation, have the capacity to enhance angiogenesis through active synthesis and release of paracrine and autocrine factors (e.g. VEGF) [64, 65]. Human MSC-derived progenies such as osteoblasts and chondrocytes are not as capable of elaborating angiogenesis when populated in microchannels of anastomized scaffolds [66]. Although the in vivo gene expression study (Fig. 8) confirmed the osteogenic differentiation of harvested scaffolds, it is possible that undifferentiated hMSCs could contribute to the increased angiogenic response through paracrine and autocrine signaling from cell-based scaffolds. Overall our in vivo data suggested that engineered scaffolds with controlled physical topography and proper biochemical environment could enable angiogenesis of cell-seeded scaffolds. Further investigation is needed to elucidate the mechanistic links through which the vascular endothelial cells and the hMSCs-derived osteoblasts on microtextured substrates interact.

5. Conclusions

We have showed for the first time that the combined effects of biochemical supplements and micro-topographical signals can synergistically generate highly functional microvascular networks for tissue engineered bone constructs in animals. Human MSCs on post microtextures cultured in the OM condition consistently expressed higher level of osteoblast-specific markers and induced greater amount of bone matrix and mineralization compared with the BM condition. The in vivo study found increased osteogenic differentiation and identified the presence of substantial amounts of microvasculature for hMSCs on the post microtextures in OM, indicating well-vascularized grafts within the host. This study demonstrates the potential advancement toward engineering vascularized cell-based bone scaffolds

through combining topographical and biochemical cues by leveraging the precision and reproducibility of microfabrication and related MEMS techniques for developing therapeutic orthopedic grafts in the future.

Disclosure

There are no competing or conflicts of interest related to the work presented in this manuscript for the authors.

Acknowledgements

This research was supported by NSF Graduate Research Fellowship (SS), Harry Wm. & Diana V. Hind Distinguished Professorship in Pharmaceutical Sciences II (SR), Annemarie and Ken Moseley, and the MTF Junior Investigator Award (CSB). We would like to thank colleagues Rachel Cheng for her assistance with some of the imaging works and Aaron Taylor for instruction on a number of the biological assays.

References

[1] Finkemeier CG. Bone-grafting and bone-graft substitutes. The Journal of bone and joint surgery American volume 2002;84-A:454-64.
[2] Van Heest A, Swiontkowski M. Bone-graft substitutes. Lancet 1999;353 Suppl 1:SI28-9.
[3] Van der Stok J, Van Lieshout EM, El-Massoudi Y, Van Kralingen GH, Patka P. Bone substitutes in the Netherlands - a systematic literature review. Acta biomaterialia 2011;7:739-50.
[4] Nandi SK, Roy S, Mukherjee P, Kundu B, De DK, Basu D. Orthopaedic applications of bone graft & graft substitutes: a review. The Indian journal of medical research 2010;132:15-30.
[5] Lee M, Song HK, Yang KH. Clinical outcomes of autogenous cancellous bone grafts obtained through the portal for tibial nailing. Injury 2012;43:1118-23.
[6] Mauffrey C, Madsen M, Bowles RJ, Seligson D. Bone graft harvest site options in orthopaedic trauma: a prospective in vivo quantification study. Injury 2012;43:323-6.
[7] Mahato NK. Characterization of cortico-cancellous bone along the iliac crest: focus on graft harvesting. Surgical and radiologic anatomy : SRA 2011;33:433-7.
[8] Pollock R, Alcelik I, Bhatia C, Chuter G, Lingutla K, Budithi C, et al. Donor site morbidity following iliac crest bone harvesting for cervical fusion: a comparison between minimally invasive and open techniques. European spine journal : official publication of the European Spine Society, the European Spinal Deformity Society, and the European Section of the Cervical Spine Research Society 2008;17:845-52.
[9] Seiler JG, 3rd, Johnson J. Iliac crest autogenous bone grafting: donor site complications. Journal of the Southern Orthopaedic Association 2000;9:91-7.
[10] Hofmann A, Konrad L, Hessmann MH, Kuchle R, Korner J, Rompe JD, et al. The influence of bone allograft processing on osteoblast attachment and function. Journal of orthopaedic research : official publication of the Orthopaedic Research Society 2005;23:846-54.
[11] Brigman BE, Hornicek FJ, Gebhardt MC, Mankin HJ. Allografts about the knee in young patients with high-grade sarcoma. Clinical orthopaedics and related research 2004:232-9.
[12] Tomanek RJ, Lotun K, Clark EB, Suvarna PR, Hu N. VEGF and bFGF stimulate myocardial vascularization in embryonic chick. The American journal of physiology 1998;274:H1620-6.

[13] Solorio L, Zwolinski C, Lund AW, Farrell MJ, Stegemann JP. Gelatin microspheres crosslinked with genipin for local delivery of growth factors. Journal of tissue engineering and regenerative medicine 2010;4:514-23.
[14] Formiga FR, Pelacho B, Garbayo E, Abizanda G, Gavira JJ, Simon-Yarza T, et al. Sustained release of VEGF through PLGA microparticles improves vasculogenesis and tissue remodeling in an acute myocardial ischemia-reperfusion model. Journal of controlled release : official journal of the Controlled Release Society 2010;147:30-7.
[15] Nakamura Y, Tensho K, Nakaya H, Nawata M, Okabe T, Wakitani S. Low dose fibroblast growth factor-2 (FGF-2) enhances bone morphogenetic protein-2 (BMP-2)-induced ectopic bone formation in mice. Bone 2005;36:399-407.
[16] Mahmud G, Campbell CJ, Bishop KJM, Komarova YA, Chaga O, Soh S, et al. Directing cell motions on micropatterned ratchets. Nat Phys 2009;5:606-12.
[17] Tzvetkova-Chevolleau T, Stephanou A, Fuard D, Ohayon J, Schiavone P, Tracqui P. The motility of normal and cancer cells in response to the combined influence of the substrate rigidity and anisotropic microstructure. Biomaterials 2008;29:1541-51.
[18] Su WT, Liao YF, Lin CY, Li LT. Micropillar substrate influences the cellular attachment and laminin expression. Journal of biomedical materials research Part A 2010;93:1463-9.
[19] Poellmann MJ, Harrell PA, King WP, Wagoner Johnson AJ. Geometric microenvironment directs cell morphology on topographically patterned hydrogel substrates. Acta biomaterialia 2010;6:3514-23.
[20] Meucci S, Tonazzini I, Beltram F, Cecchini M. Biocompatible noisy nanotopographies with specific directionality for controlled anisotropic cell cultures. Soft Matter 2012;8:1109-19.
[21] Mata A, Kim EJ, Boehm CA, Fleischman AJ, Muschler GF, Roy S. A three-dimensional scaffold with precise micro-architecture and surface micro-textures. Biomaterials 2009;30:4610-7.
[22] Santos MI, Reis RL. Vascularization in bone tissue engineering: physiology, current strategies, major hurdles and future challenges. Macromolecular bioscience 2010;10:12-27.
[23] Kaully T, Kaufman-Francis K, Lesman A, Levenberg S. Vascularization--the conduit to viable engineered tissues. Tissue engineering Part B, Reviews 2009;15:159-69.
[24] Nguyen LH, Annabi N, Nikkhah M, Bae H, Binan L, Park S, et al. Vascularized bone tissue engineering: approaches for potential improvement. Tissue engineering Part B, Reviews 2012;18:363-82.
[25] Khademhosseini A, Langer R, Borenstein J, Vacanti JP. Microscale technologies for tissue engineering and biology. Proceedings of the National Academy of Sciences of the United States of America 2006;103:2480-7.
[26] Norman JJ, Desai TA. Control of cellular organization in three dimensions using a microfabricated polydimethylsiloxane - Collagen composite tissue scaffold. Tissue Eng 2005;11:378-86.
[27] Holle AW, Engler AJ. More than a feeling: discovering, understanding, and influencing mechanosensing pathways. Curr Opin Biotech 2011;22:648-54.
[28] Choi CK, Breckenridge MT, Chen CS. Engineered materials and the cellular microenvironment: a strengthening interface between cell biology and bioengineering. Trends Cell Biol 2010;20:705-14.
[29] Ross AM, Jiang ZX, Bastmeyer M, Lahann J. Physical Aspects of Cell Culture Substrates: Topography, Roughness, and Elasticity. Small 2012;8:336-55.
[30] Clark P, Connolly P, Curtis AS, Dow JA, Wilkinson CD. Topographical control of cell behaviour: II. Multiple grooved substrata. Development 1990;108:635-44.
[31] Engler AJ, Griffin MA, Sen S, Bonnemann CG, Sweeney HL, Discher DE. Myotubes differentiate optimally on substrates with tissue-like stiffness: pathological implications for soft or stiff microenvironments. The Journal of cell biology 2004;166:877-87.
[32] Engler AJ, Sen S, Sweeney HL, Discher DE. Matrix elasticity directs stem cell lineage specification. Cell 2006;126:677-89.

[33] Li W, Jiang K, Ding S. Concise review: A chemical approach to control cell fate and function. Stem Cells 2012;30:61-8.
[34] Meyle J, Wolburg H, von Recum AF. Surface micromorphology and cellular interactions. Journal of biomaterials applications 1993;7:362-74.
[35] Walboomers XF, Croes HJ, Ginsel LA, Jansen JA. Growth behavior of fibroblasts on microgrooved polystyrene. Biomaterials 1998;19:1861-8.
[36] Raghavan S, Chen CS. Micropatterned environments in cell biology. Adv Mater 2004;16:1303-13.
[37] Chen CS, Jiang XY, Whitesides GM. Microengineering the environment of mammalian cells in culture. Mrs Bull 2005;30:194-201.
[38] Roy S, Ferrara LA, Fleischman AJ, Benzel EC. Microelectromechanical systems and neurosurgery: A new era in a new millennium. Neurosurgery 2001;49:779-97.
[39] Hamilton DW, Wong KS, Brunette DM. Microfabricated discontinuous-edge surface topographies influence osteoblast adhesion, migration, cytoskeletal organization, and proliferation and enhance matrix and mineral deposition in vitro. Calcified Tissue Int 2006;78:314-25.
[40] Dalby MJ, Gadegaard N, Tare R, Andar A, Riehle MO, Herzyk P, et al. The control of human mesenchymal cell differentiation using nanoscale symmetry and disorder. Nat Mater 2007;6:997-1003.
[41] Fu J, Wang YK, Yang MT, Desai RA, Yu X, Liu Z, et al. Mechanical regulation of cell function with geometrically modulated elastomeric substrates. Nature methods 2010;7:733-6.
[42] McBeath R, Pirone DM, Nelson CM, Bhadriraju K, Chen CS. Cell shape, cytoskeletal tension, and RhoA regulate stem cell lineage commitment. Developmental cell 2004;6:483-95.
[43] Kim EJ, Fleischman AJ, Muschler GF, Roy S. Response of bone marrow derived connective tissue progenitor cell morphology and proliferation on geometrically modulated microtextured substrates. Biomed Microdevices 2013;15:385-96.
[44] Walboomers XF, Jansen JA. Microgrooved silicone subcutaneous implants in guinea pigs. Biomaterials 2000;21:629-36.
[45] Walboomers XF, Croes HJ, Ginsel LA, Jansen JA. Microgrooved subcutaneous implants in the goat. Journal of biomedical materials research 1998;42:634-41.
[46] Meyle J, Gultig K, Nisch W. Variation in contact guidance by human cells on a microstructured surface. Journal of biomedical materials research 1995;29:81-8.
[47] Schmittgen TD, Livak KJ. Analyzing real-time PCR data by the comparative C(T) method. Nature protocols 2008;3:1101-8.
[48] Fujii M, Takeda K, Imamura T, Aoki H, Sampath TK, Enomoto S, et al. Roles of bone morphogenetic protein type I receptors and Smad proteins in osteoblast and chondroblast differentiation. Molecular biology of the cell 1999;10:3801-13.
[49] Hall BK. The role of movement and tissue interactions in the development and growth of bone and secondary cartilage in the clavicle of the embryonic chick. Journal of embryology and experimental morphology 1986;93:133-52.
[50] Rasmussen AS, Lauridsen H, Laustsen C, Jensen BG, Pedersen SF, Uhrenholt L, et al. High-resolution ex vivo magnetic resonance angiography: a feasibility study on biological and medical tissues. BMC physiology 2010;10:3.
[51] Colnot C, Romero DM, Huang S, Helms JA. Mechanisms of action of demineralized bone matrix in the repair of cortical bone defects. Clinical orthopaedics and related research 2005:69-78.
[52] Discher DE, Janmey P, Wang YL. Tissue cells feel and respond to the stiffness of their substrate. Science 2005;310:1139-43.
[53] Vogel V, Sheetz M. Local force and geometry sensing regulate cell functions. Nature reviews Molecular cell biology 2006;7:265-75.
[54] Goodman SL, Sims PA, Albrecht RM. Three-dimensional extracellular matrix textured biomaterials. Biomaterials 1996;17:2087-95.

[55] Abrams GA, Goodman SL, Nealey PF, Franco M, Murphy CJ. Nanoscale topography of the basement membrane underlying the corneal epithelium of the rhesus macaque. Cell Tissue Res 2000;299:39-46.
[56] Wang L, Sun B, Ziemer KS, Barabino GA, Carrier RL. Chemical and physical modifications to poly(dimethylsiloxane) surfaces affect adhesion of Caco-2 cells. Journal of biomedical materials research Part A 2010;93:1260-71.
[57] Stein GS, Lian JB. Molecular mechanisms mediating proliferation/differentiation interrelationships during progressive development of the osteoblast phenotype. Endocrine reviews 1993;14:424-42.
[58] Aubin JE. Bone stem cells. Journal of cellular biochemistry Supplement 1998;30-31:73-82.
[59] Chen JK, Shapiro HS, Wrana JL, Reimers S, Heersche JN, Sodek J. Localization of bone sialoprotein (BSP) expression to sites of mineralized tissue formation in fetal rat tissues by in situ hybridization. Matrix 1991;11:133-43.
[60] Nefussi JR, Brami G, Modrowski D, Oboeuf M, Forest N. Sequential expression of bone matrix proteins during rat calvaria osteoblast differentiation and bone nodule formation in vitro. The journal of histochemistry and cytochemistry : official journal of the Histochemistry Society 1997;45:493-503.
[61] Millan JL. Alkaline Phosphatases : Structure, substrate specificity and functional relatedness to other members of a large superfamily of enzymes. Purinergic signalling 2006;2:335-41.
[62] Marks Jr SC, Odgren PR. Chapter 1 - Structure and Development of the Skeleton. In: Rodan JPBGRA, editor. Principles of Bone Biology (Second Edition). San Diego: Academic Press; 2002. p. 3-15.
[63] Kenneth Ward W. A review of the foreign-body response to subcutaneously-implanted devices: the role of macrophages and cytokines in biofouling and fibrosis. Journal of diabetes science and technology 2008;2:768-77.
[64] Caplan AI, Dennis JE. Mesenchymal stem cells as trophic mediators. J Cell Biochem 2006;98:1076-84.
[65] Tang YL, Zhao Q, Zhang YC, Cheng LL, Liu MY, Shi JH, et al. Autologous mesenchymal stem cell transplantation induce VEGF and neovascularization in ischemic myocardium. Regul Peptides 2004;117:3-10.
[66] Lee CH, Marion NW, Hollister S, Mao JJ. Tissue Formation and Vascularization in Anatomically Shaped Human Joint Condyle Ectopically in Vivo. Tissue Eng Pt A 2009;15:3923-30.

Figure Legends and Tables

Table 1. A list of primers used in RT-PCR analysis of in vitro and in vivo microtextured scaffolds.

Table 2. A list of primers used in RT-PCR analysis of in vivo cell-cultured microtextured scaffolds.

Table 3. The number of harvested scaffolds with vascular formation based on a double-blind observation.

Figure 1. Fabrication of PDMS post microtextures by soft lithography. Briefly, 10 μm thick SU-8 2010 photoresist was spin coated on top of silicon wafers. The post microtexture pattern with 10 μm inter-space was transferred from a photomask onto the photoresist under UV exposure. The liquid PDMS and curing photocatalyst were mixed at a ratio of 10:1, degassed for 20 min, and then poured uniformly on top of the patterned mold. The PDMS substrates were cured at 85 ℃ for 2 h.

Figure 2. Number of cells on PDMS microtextured substrates in basal medium (BM) and osteogenic medium (OM) for 6 weeks. The positive control mouse pre-osteoblast cell lines calB2T3 and MC3T3 and hMSCs were cultured on microtextured substrates. Proliferation study showed that hMSCs have less proliferative capacity than the positive controls in both BM and OM conditions. The number of hMSCs on microtextured surfaces increased significantly in BM compared to OM. (n>3, *p<0.05, **p<0.005, ****p<0.0001)

Figure 3. SEM images of hMSCs on PDMS microtextured substrates for 6 weeks. (a) PDMS post microtexture. (b) hMSCs on PDMS microtextured substrates in BM. (c) hMSCs on PDMS microtextured substrates in OM. On microtextured substrates in BM (d), hMSCs mostly tended to attach next to the posts and spread their processes towards posts and other cells (white arrows). hMSCs on microtextured substrates in OM (e) showed cell spreading over the top of the microposts and coverage with ECM (black arrows) on the substrate surfaces.

Figure 4. RT-PCR analysis of hMSCs on microtextured substrates in BM and OM. Relative gene expression of hMSCs on microtextured substrates in BM and OM compared to the negative controls, hMSCs cultured in BM (a) and hMSCs cultured in OM (b) on smooth surface. Relative gene expression of hMSCs on microtextured substrates in BM and OM compared to the positive control, human osteosarcoma cell line Saos-2 on smooth surface (c). The PDMS microtextured substrates enhanced the osteogenic differentiation of hMSCs in the proliferative basal medium (BM) condition as indicated by the high levels of expression in osteogenic markers (COL I, ALP, BSP, and OC) (a,b). The osteogenic differentiation of hMSCs on microtextured substrates was further elevated by culturing under the differentiative osteogenic medium (OM) (a,b). The expression of BSP, an early marker of osteoblast differentiation, and OC, a marker of late-stage differentiation, were significantly enhanced for hMSCs on microtextured substrates in BM and OM compared to the positive control human osteosarcoma cell line Saos-2 (c), affirming the effectiveness of using microtextured substrates and biochemical supplements to promote late-stage bone differentiation. (n>3, *p<0.05)

Figure 5. Alkaline phosphatase levels were normalized for cells cultured on microtextured surfaces in basal medium (BM) and osteogenic medium (OM). The level of mineralization enhanced significantly for hMSCs on microtextured substrates in OM compared to BM. The positive control pre-osteoblast cell lines calB2T3 and MC3T3 showed a greater level of mineralization in both BM and OM. (n=3, **p<0.005)

Figure 6.Vasculature observed from harvested scaffolds after a 6-week implantation in mice. (a) microtextured substrates without hMSCs. (b) hMSCs on microtextured surfaces in BM. (c,d) hMSCs on microtextured surfaces in OM. Microtextured substrates without hMSCs (a) that were implanted in mice lacked any microvasculature and integration with the surrounding host tissues. hMSCs on microtextured surfaces in BM (b) exhibited micro-vessel

growth surrounding the edge of the substrates, whereas hMSCs on microtextured surfaces in OM (c,d) showed a more perfused and extensive network of blood vessels in all directions.

Figure 7. SEM images of harvested scaffolds after a 6-week implantation in mice. (a,b) microtextured substrates without hMSCs. (c,d) hMSCs on microtextured surfaces in BM. (e,f) hMSCs on microtextured surfaces in OM. All implanted scaffolds developed ECM rich capsules with uniform shape and thickness around the entire microtextured substrates. However, the sprouting of new blood vessels [50] in tissue surrounding the implants was significantly higher for hMSCs on microtextured surfaces in OM (e,f). Red blood cells (black arrows) were observed for implants of hMSCs on microtextured surfaces in OM (e,f).

Figure 8. RT-PCR analysis of harvested scaffolds after a 6-week implantation in mice. (a) The expression of osteogenic markers (COL I, COL X, ALP, BSP, and OC) were determined for blank microtextured substrates (PDMS) without hMSCs, hMSCs on microtextured surface in basal medium (hMSCs + PDMS in BM), and hMSCs on microtextured surface in osteogenic medium (hMSCs + PDMS in OM). (b) The expression of angiogenic markers (PECAM and VEGF) were measured for blank microtextured substrates (PDMS), hMSCs on microtextured surface in basal medium (hMSCs + PDMS in BM), and hMSCs on microtextured surface in osteogenic medium (hMSCs + PDMS in OM). Gene analysis of harvested implants demonstrated that hMSCs on microtextured surfaces in OM (hMSCs + PDMS in OM) provided the optimal condition to accelerate the early and late stage of hMSCs osteogenesis in vivo. hMSCs on microtextured surfaces in OM (hMSCs + PDMS in OM) also promoted vascularization based on the increased expression of angiogenic makers, indicating successful integration of vascularized osteogenic bone grafts. ($n>3$, $*p<0.05$, $***p<0.001$)

Figure 9. Immunofluorescence staining of osteogenic markers COL I (red, b,f,j) and OC (green, c,g,k) for harvested scaffolds after a 6-week implantation. Nuclei were stained with DAPI (d,h,l). *(Note: the original color images were converted to grayscale and reversed to provide visual clarity.)* (a-d) microtextured substrates without hMSCs. (e-h) hMSCs on microtextured surfaces in BM. (i-l) hMSCs on microtextured surfaces in OM (i-l). Blank microtextured substrates showed minimal cell attachment on the surface (d) and exhibited no COL I and OC stainings (b,c). hMSCs on microtextured surfaces in BM (f,g) and OM (j,k) revealed high intensity of COL I and OC compared to the negative control blank microtextured substrates (b,c), indicating the differentiation of hMSCs toward osteogenic lineage on microtextured surfaces in vivo.

Figure 10. Immunofluorescence staining of human mitochondria (green, e,d,g) and mouse PECAM (red, b,e,h) for harvested scaffolds after a 6-week implantation. Nuclei were stained with DAPI (c,f,i). *(Note: the original color images were converted to grayscale and reversed to provide visual clarity.)* (a-c) microtextured substrates without hMSCs. (d-f) hMSCs on microtextured surfaces in BM. (g-i) hMSCs on microtextured surfaces in OM. Blank microtextured substrates without hMSCs showed minimal cell attachment on the surface (c) and exhibited neither human nor mouse markers (a,b). hMSCs on microtextured surfaces in BM (d,e) and OM (g,h) revealed elevated signals of human mitochondria and mouse PECAM compared to the negative control blank microtextured substrates without hMSCs (a,b), which confirmed the presence of hMSCs on the microtextured surfaces and identified mouse blood vessels attracted to the scaffolds.

Figure 11. Alkaline phosphatase levels were determined in harvested scaffolds after a 6-week implantation. hMSCs on microtextured surfaces in basal medium (BM) and osteogenic medium (OM) demonstrated bone matrix mineralization characterized by an increased level of alkaline phosphatase activity in vivo. ($n=3$, $**p<0.005$, $*p<0.05$)

Figure 12. Cross-sectional images of HE staining for harvested scaffolds after a 6-week implantation. (a) microtextured substrates without hMSCs. (b) hMSCs on microtextured substrates in BM. (c-e) hMSCs on microtextured substrates in OM. Microtextured substrates were shredded into PDMS pieces during HE sectioning (a). No stained tissue debris detected for microtextured substrates (a). hMSCs on microtextured substrates in BM (b)

showed densely nucleated epithelial layers surrounding the substrates, whereas hMSCs on microtextured substrates in OM (c-e) exhibited very loose tissues accompanied by extensive blood vessels (black arrows). Blood (red arrows) was also observed in the vascular lumen for hMSCs on microtextured substrates in OM (c-e).

Figure S1. Immunofluorescence staining of osteogenic markers COL I (red, b,f,j) and OC (green, c,g,k) on microtextured scaffolds. Nuclei were stained with DAPI (d,h,l). *(Note: the original color images were converted to grayscale and reversed to provide visual clarity.)* (a-d) hMSCs on smooth PDMS substrates. (e-h) hMSCs on microtextured surfaces in BM. (i-l) hMSCs on microtextured surfaces in OM (i-l). hMSCs on microtextured surfaces in BM (f,g) and OM (j,k) revealed high intensity of COL I and OC compared to the negative control, undifferentiated hMSCs on smooth surface (b,c), indicating the differentiation of hMSCs toward osteogenic lineage.

Figure S2. Alizarin red staining of cells cultured on microtextured surfaces in basal medium (BM) (a-d) and osteogenic medium (OM) (e-h). (a,e) microtextured substrates. (b,f) calB2T3 on microtextured surfaces. (c,g) MC3T3 on microtextured surfaces. (d,h) hMSCs on microtextured surfaces. The OM condition (f-h) enhanced calcium deposition of cells on microtextured surfaces compared to the BM condition (b-d). hMSCs on microtextured substrates in both BM (d) and OM (h) showed significant amount of calcium deposition.

Figure S3. Alizarin red staining of harvested scaffolds after a 6-week implantation. (a,d) microtextured substrates without hMSCs. (b,e) hMSCs on microtextured surfaces in BM. (c,f) hMSCs on microtextured surfaces in OM. The microtextured substrates showed minimal calcium deposition on top of the substrate surfaces. hMSCs on microtextured surfaces in BM (b,e) and OM (c,f) showed significant amount of calcium deposition characterized by the amount of red staining, indicating the successful differentiation of hMSCs toward osteogenic lineage.

Figure S4. Cross-sectional HE staining of harvest scaffolds after a 6-week implantation. (a) hMSCs on microtextured substrates in BM. (b) hMSCs on microtextured substrates in OM. hMSCs on microtextured substrates in BM (a) exhibited dense epithelial-like tissue surrounding the scaffolds, while hMSCs on microtextured substrates in OM (b) showed loose tissue structure and blood vessels.

Figure 1.

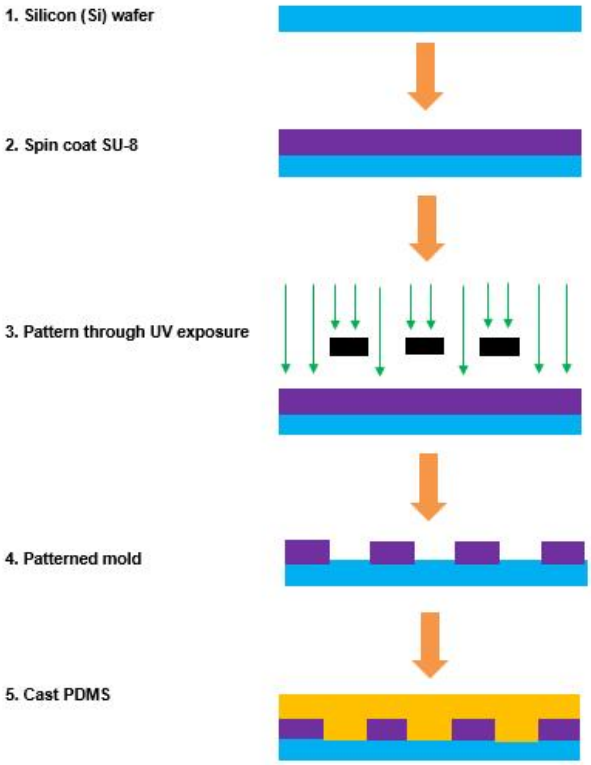

Figure 2.

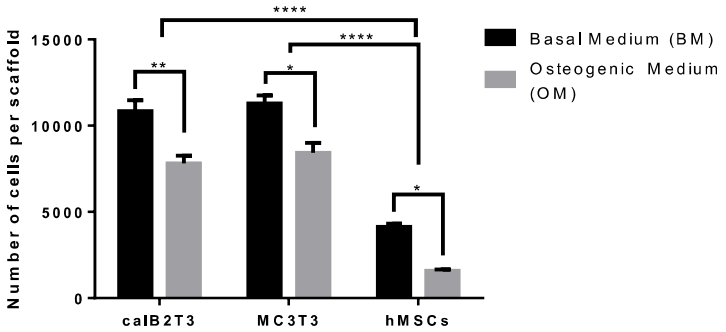

Figure 3.

a. **Microtexture**

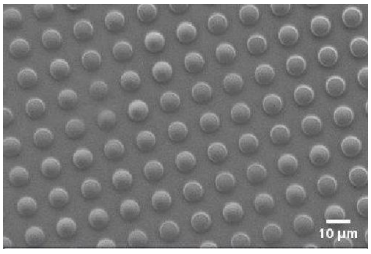

b. **hMSCs in BM**

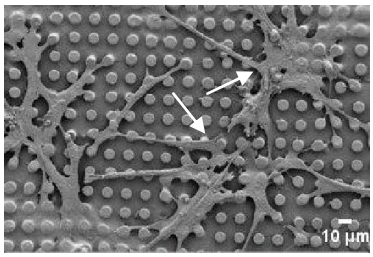

c. **hMSCs in OM**

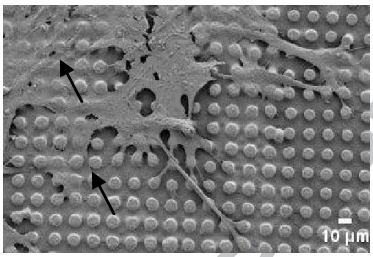

Figure 4.

a. **hMSCs in BM on smooth surface as negative control**

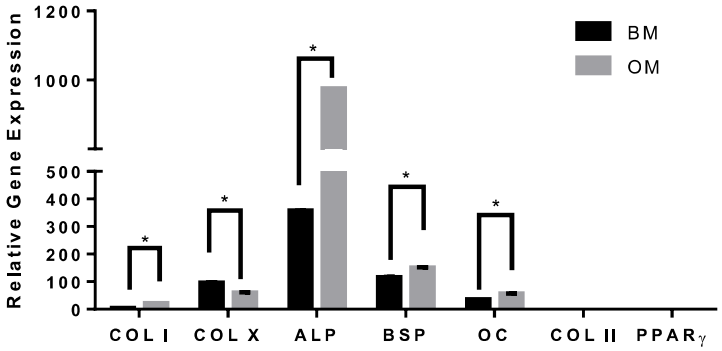

b. **hMSCs in OM on smooth surface as negative control**

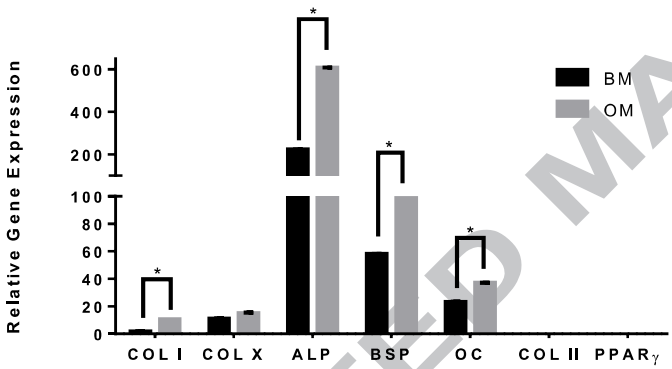

c. **Human Saos-2 on smooth surface as positive control**

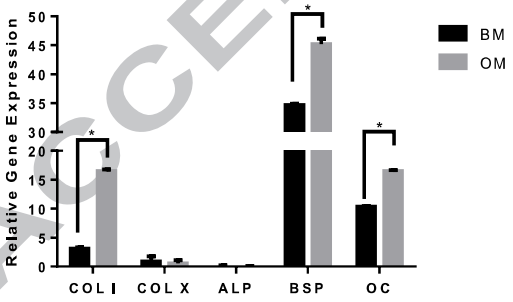

Figure 5.

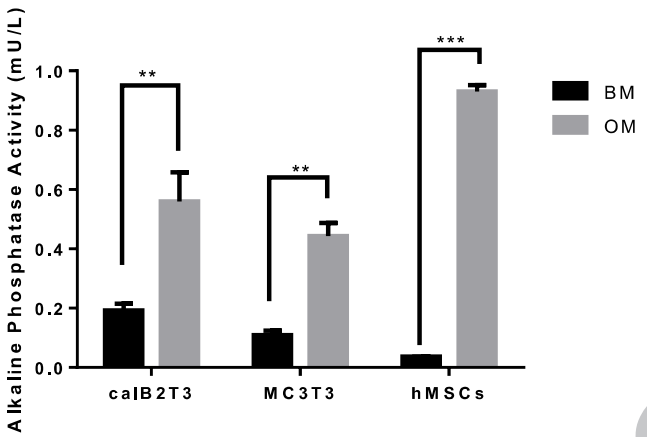

Figure 6.

a. **Microtexture**

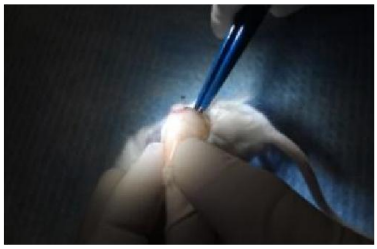

b. **hMSCs in BM**

c. **hMSCs in OM**

d. **hMSCs in OM**

Figure 7.

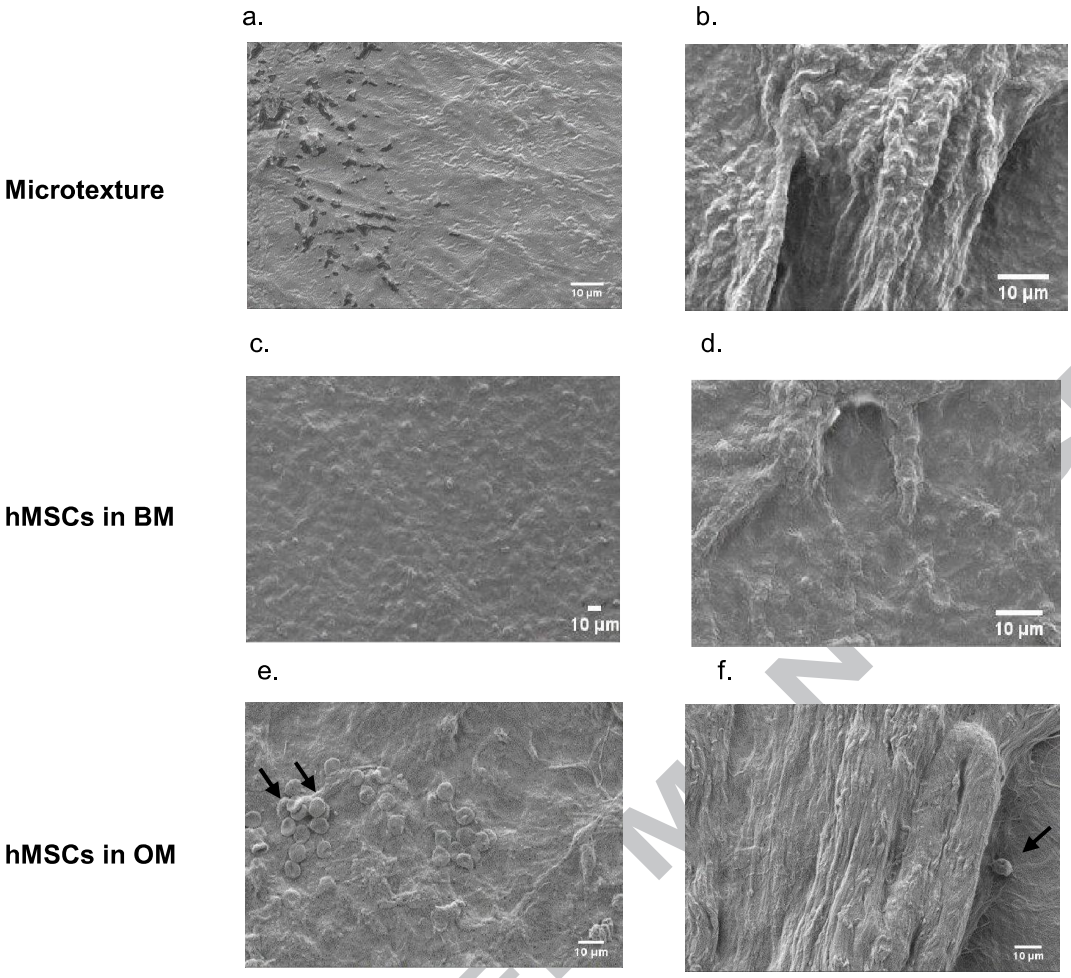

Figure 8.

a. **RT-PCR analysis of osteoblast-specific markers**

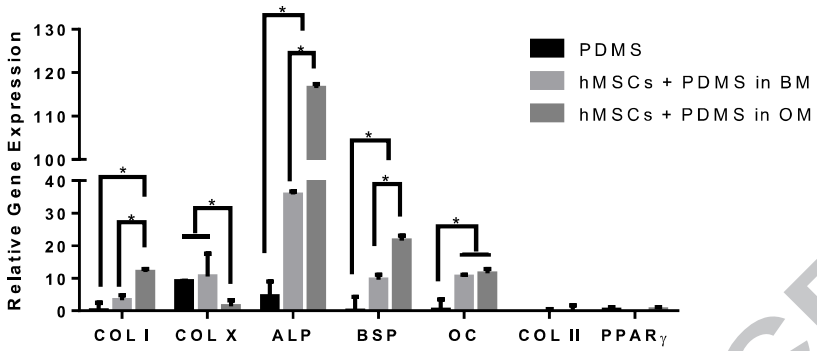

b. **RT-PCR analysis of angiogenic-specific markers**

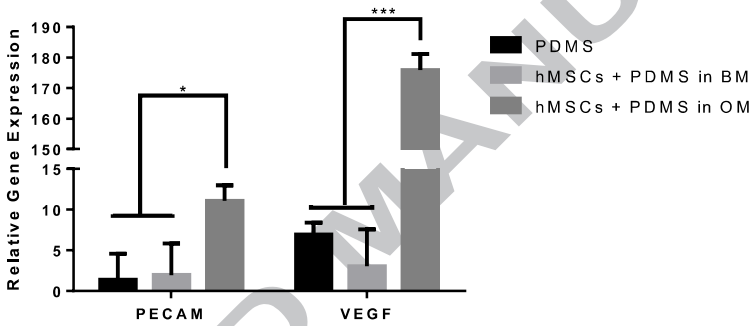

Figure 9.

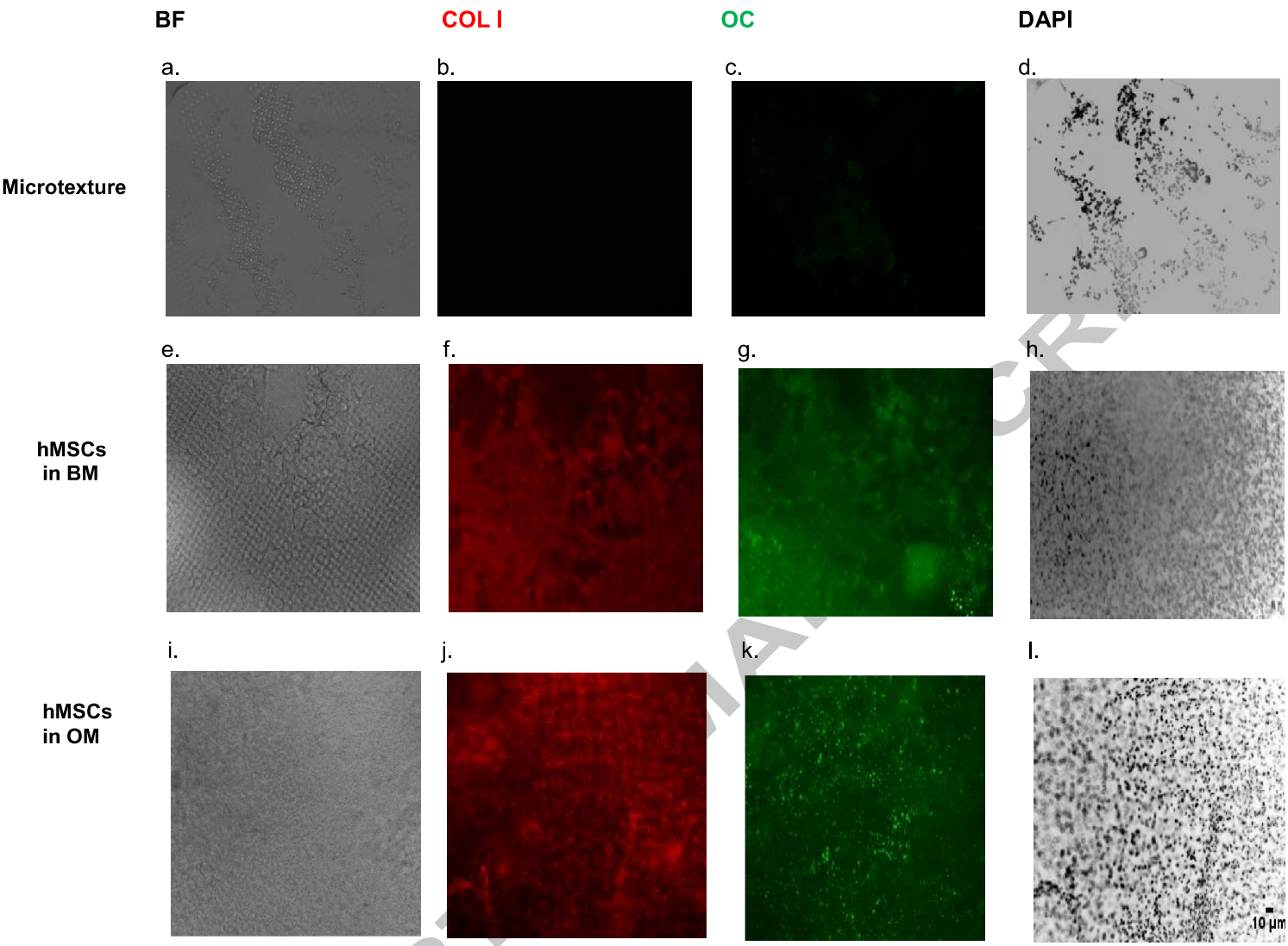

Figure 10.

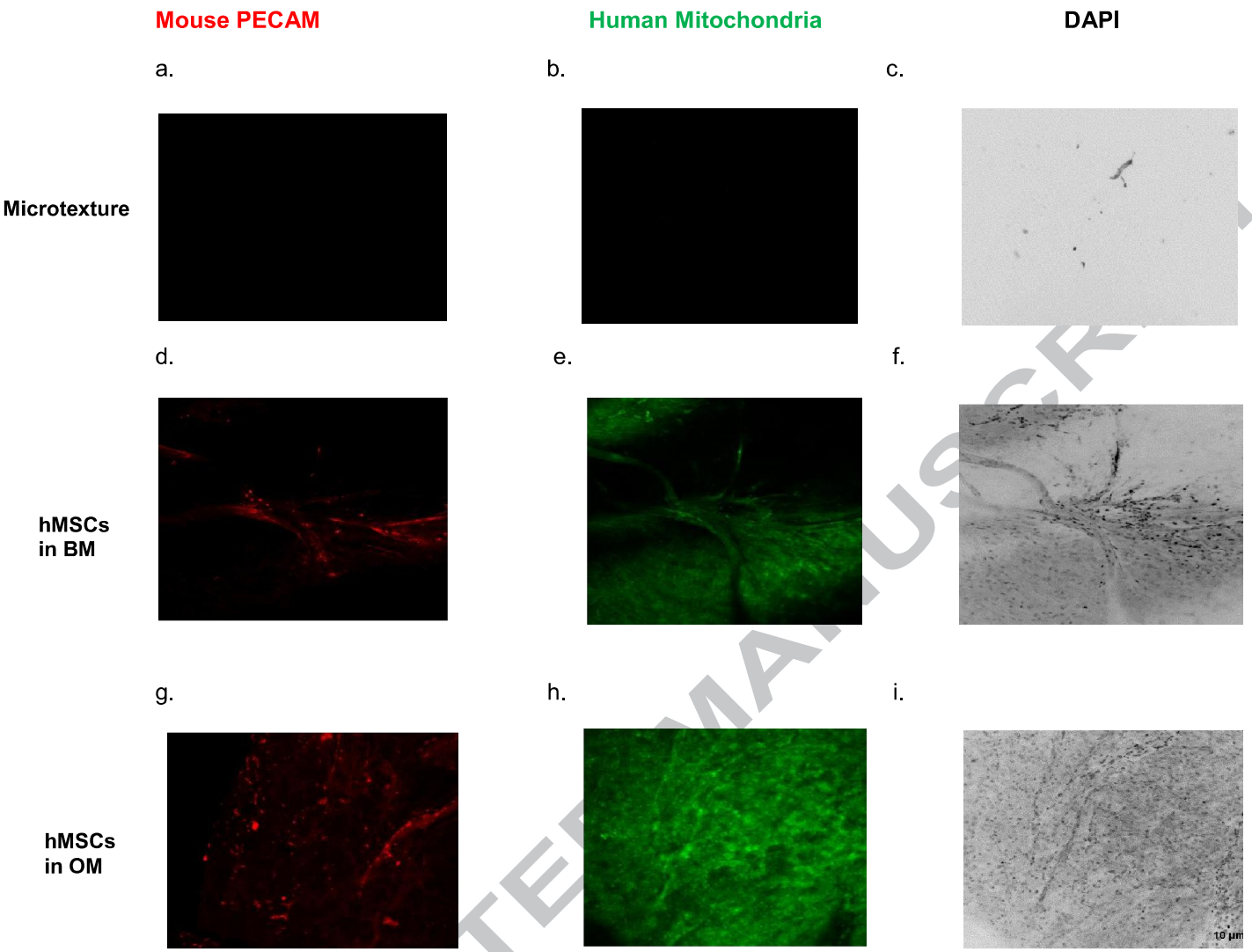

Figure 11.

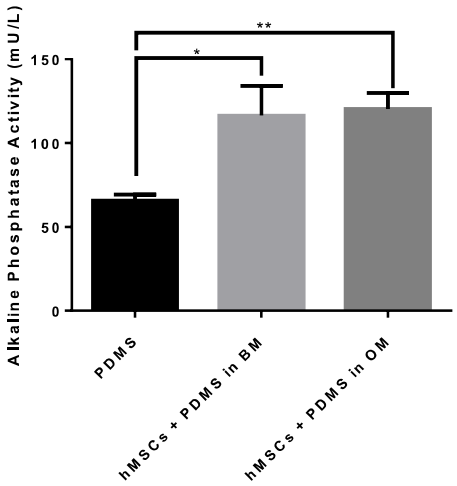

Figure 12.

a. **Microtexture**

b. **hMSCs in BM**

c. **hMSCs in OM**

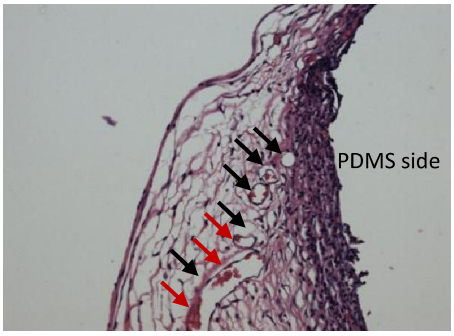

d. **hMSCs in OM**

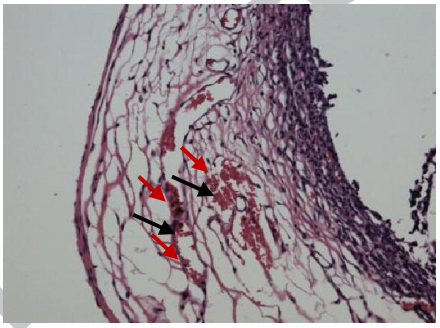

e. **hMSCs in OM**

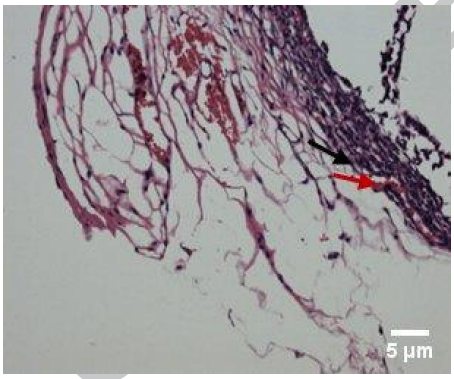

Table 1.

Species	Gene Makers	Forward (5'-3')	Reverse (5'-3')
Human	COL I	CAGCCGCTTCACCTACAGC	TTTTGTATTCAATCACTGTCTTGCC
	COL X	CAAGGCACCATCTCCAGGAA	AAAGGGTATTTGTGGCAGCATATT
	ALP	ACGTGGCTAAGAATGTCATC	CTGGTAGGCGATGTCCTTA
	BSP	CATTTTGGGAATGGCCTGTG	ATTGTCTCCGCTGCTGC
	OC	GAAGCCCAGCGGTGCA	CACTACCTCGCTGCCCTCC
	COL II	TATGCCAACTTCCCACACG	AAGGCACCTTGTAAGACCTAGAC
	PPARγ	CCAGATGCCAACTTCCCACACG	AAGGCACCTTGTAAGACCTAGAC
	GAPDH	ATGGGGAAGGTGAAGGTC	TAAAAGCAGCCCTGGTGACC

Table 2.

Species	Gene Makers	Forward (5'-3')	Reverse (5'-3')
Mouse	PECAM	TGCTCTCGAAGCCCAGTATT	CGCTGAACACCGCGGGGTGGGAATGGC
	VEGF	GGAGATCCTTCGAGGAGCACTT	GGCGATTTAGCAGCAGATATAAGAA
	GAPDH	TGCCCCCATGTTTGTGATG	TGTGGTCATGAGCCCTTCC

Table 3.

Sample	Overall Vascularization	Edge Vascularization	No Vascularization
PDMS	1	--	2
hMSCs + PDMS in BM	2	2	--
hMSCs + PDMS in OM	4	--	--